ACS Catalysis

Research Article

pubs.acs.org/acscatalysis

Organometallic Preparation of Ni, Pd, and NiPd Nanoparticles for the Design of Supported Nanocatalysts

Natalia J. S. Costa,[†,§] Miguel Guerrero,[§] Vincent Collière,[§] Érico Teixeira-Neto,[†] Richard Landers,[‡] Karine Philippot,*[,§] and Liane M. Rossi*[,†]

[†]Departamento de Química Fundamental, Instituto de Química, Universidade de São Paulo, 05508-000 São Paulo, SP, Brazil

[§]CNRS, LCC (Laboratoire de Chimie de Coordination), Université de Toulouse; UPS, INPT; LCC, 205, route de Narbonne, F-31077 Toulouse cedex 4, France

[‡]Instituto de Física, UNICAMP, 13083-970 Campinas, SP, Brazil

ABSTRACT: The preparation of bimetallic nanoparticles with controlled size, shape, and composition remains a difficult task, and reproducible methods are highly desired. Here, we report the codecomposition of $Ni(cod)_2$ and $Pd_2(dba)_3$ organometallic precursors in the presence of hexadecylamine (HDA) and hydrogen as an efficient approach to get size-controlled bimetallic nickel–palladium nanoparticles. Presynthesized nickel–palladium nanoparticles of different Ni/Pd ratios were further used for the preparation of supported catalysts by the sol–immobilization method onto a magnetic silica. The obtained supported catalysts were investigated in the hydrogenation of cyclohexene and compared to Ni and Pd monometallic catalysts. The catalysts prepared with a 1:9 Ni/Pd molar ratio achieved the highest initial turnover frequency > 50 000 h^{-1}, providing higher activity than the pure Pd monometallic counterpart. This represents an important saving of noble metal. Moreover, the magnetic separation allows excellent separation of the catalyst from the liquid products without metal leaching and exposure to air, leading to an efficient recycling.

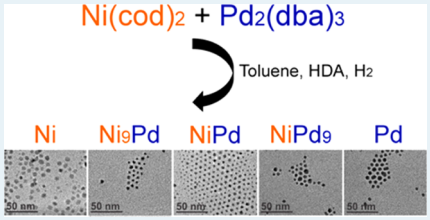

KEYWORDS: *organometallic synthesis, bimetallic nanoparticles, monometallic nanoparticles, nickel, palladium, hydrogenation, magnetic separation*

1. INTRODUCTION

Metal nanoparticles are attractive materials in many fields ranging from physics (hard or soft magnetic materials; optics; microelectronics) to catalysis.[1,2] In catalysis, metal nanoparticles are receiving considerable interest due to their strong potential (high number of active surface sites) which has long been used in heterogeneous catalysis (heterogeneous catalysts for difficult hydrogenations, electrocatalysts for fuel cells), but which also appears promising in the solution phase.[3−11]

Among others, bimetallic nanoparticles constitute an important class of nanocatalysts due to the high number of possibilities for varying the structure and composition toward designing new properties.[12] Bimetallic nanoparticles are usually classified on the basis of the chemical distribution of the two metals in the particles. For example, one can distinguish bimetallic alloys characterized by the formation of a statistical distribution of the two elements, metallic solid solutions, or hetero/core–shell nanostructures, which contain segregated domains of both metals. Synergistic effects are expected to arise from the presence of the two metals and the intimate contact between them.[13−15]

Most of the solution-phase methods for preparing metal nanoparticles to be applied in catalysis involve the use of metal salt precursors under reducing conditions.[16−20] Nevertheless, the decomposition of organometallic precursors has emerged as an efficient and reproducible approach toward the preparation of well-controlled metal nanoparticles in terms of dispersion, size distribution, and composition.[21] The nanoparticles obtained using this method are suitable for meaningful studies of their morphology–property relationships.[22]

Preferable precursors are based on olefinic organometallic complexes that decompose easily under a dihydrogen atmosphere, via hydrogenation of the olefinic ligands, into corresponding alkanes that are inert toward the metallic surface.[22] Thus, metal nanoparticles with a surface free of contaminants from metal precursors or reducing agents are produced; this is a great advantage if one wants to deeply explore their surface chemistry, because the only molecules present on the surface are the polymers or ligands used for their stabilization. As a result, the organometallic approach has also been considered to be suitable for preparing nanomaterials for catalytic applications that can benefit from clean metal surfaces or from functionalized ones, when choosing specific stabilizing ligands.[22,23]

Organometallic synthesis can be employed to prepare metal nanocatalysts in solution (colloidal suspensions), as well as to obtain supported catalysts using various inorganic solids as their supports.[24−27] Supported metal nanoparticles are usually more

Received: March 14, 2014
Revised: April 11, 2014
Published: April 14, 2014

suitable for catalytic applications than nanoparticles in colloidal suspensions not only because of their easy separation but also due to the beneficial interactions between the nanoparticles and the support that can improve the catalytic activity, compared to the pristine metal nanoparticles in solution.[28−30]

The preparation of supported nanocatalysts can be performed by simple impregnation of a chosen support with a colloidal suspension containing preformed nanoparticles[25] (also called the sol−immobilization method) or by the direct synthesis of supported nanoparticles by the decomposition of an organometallic complex in the presence of a solid support.[31] This second way appears as a simplified "one-pot" procedure, which consists of adding an organometallic precursor solution to a solid support and then submitting the mixture to molecular hydrogen pressure to induce the formation of the particles in the presence of the support. For example, the organometallic complexes bis(cyclooctadiene)-nickel(0) [$Ni(cod)_2$] and tris-(dibenzylideneacetone)-dipalladium(0) [$Pd_2(dba)_3$] were used to prepare supported Ni(0)[32] and Pd(0)[33] nanoparticles as catalysts for hydrogenation reactions. The Ni(0) catalyst prepared from $Ni(cod)_2$ was resistant to oxidation; most of the sample remained as Ni(0), even after storage in air, and only partial surface oxidation occurred. Additionally, the surface-oxidized nickel species could be reduced back to Ni(0), the catalyst's active form, under very mild hydrogenation reaction conditions (1 bar of dihydrogen at 75 °C). The so-obtained nanocatalyst exhibited high activity in the hydrogenation of cyclohexene and could be recycled 15 times without deactivating (TOF up to 1500 h^{-1}, 75 °C, and 6 atm of dihydrogen).[32] The catalytic properties were excellent, but this method provided nickel aggregates instead of size-controlled nanoparticles.

We report, here, the preparation of supported Ni, Pd, and bimetallic NiPd nanoparticles by immobilization of preformed nanoparticles onto a magnetic silica support (sol−immobilization method). The colloidal nickel−palladium nanoparticles were synthesized by the simultaneous decomposition of $Ni(cod)_2$ and $Pd_2(dba)_3$ in the presence of hexadecylamine (HDA) as stabilizer. The so-obtained nanomaterials were tested as catalysts for the hydrogenation of cyclohexene, providing a comparative study of the relationships between structure and activity.

2. EXPERIMENTAL SECTION

2.1. General Procedures. The synthesis of the nanocatalysts and the catalytic experiments were carried out under an argon or dinitrogen atmosphere using vacuum line techniques or a glovebox. The reactions were performed with standard Schlenk tubes or Fischer−Porter glass reactors. Toluene was purchased from SDS and dried through a purification machine (MBraun MB SPS-800). Cyclohexene (Sigma-Aldrich) was dried with $MgSO_4$ and distilled under a dinitrogen atmosphere. The solvents were used immediately after drying.

The synthesis of the catalyst support was carried out under air conditions. MeOH (99.8%) was purchased from Synth, and NH_4OH (28%) was purchased from J.T. Baker. The reagents were of analytical grade and commercially available (Aldrich), including $Ni(cod)_2$. $Pd_2(dba)_3$ was purchased from Strem Chemicals.

2.2. Catalyst Preparation. The following notation is used for the catalyst samples prepared in this study: FFSi denotes the catalyst support, and x and y denote the Ni and Pd molar ratios, respectively.

2.2.1. Preparation of Ni_xPd_y Nanoparticles. A mixture of $Ni(cod)_2$ and $Pd_2(dba)_3$, containing 0.9 mmol of metal (nickel and palladium) in different molar ratios of Ni/Pd (1:0, 9:1, 1:1, 1:9, and 0:1), was introduced into a Fischer−Porter glass reactor under an argon atmosphere. A solution of hexadecylamine in toluene (30 mL, 0.3 mol·L^{-1}) was then transferred under an argon atmosphere to the Fischer−Porter reactor immersed in an ethanol/liquid nitrogen bath containing the organometallic precursors. The mixture was submitted to a vacuum to remove the argon and then pressurized under dihydrogen (3 bar).

The cold bath was removed and the mixture was vigorously stirred until reaching room temperature (r.t.). The reactor was submerged in an oil bath at 110 °C, and the mixture was stirred for 20 h, leading to the formation of the bimetallic nanoparticles. These solutions of Ni_xPd_y were used as obtained for the preparation of supported catalysts by the sol−immobilization method detailed in Section 2.2.2.

The nanoparticles were purified to compare their catalytic activity with the supported colloidal nanoparticles. The solution of Ni_xPd_y in the Fischer−Porter reactor was concentrated to 5 mL under vacuum conditions. The resulting suspension was immersed in an ice bath, and 30 mL of cold pentane was then added to precipitate the nanoparticles. The supernatant was removed with a syringe, and the solid was washed 5 times with 30 mL of cold pentane, giving rise to purified nanoparticles.

2.2.2. Sol−Immobilization of Ni_xPd_y Nanoparticles. The catalysts supported on the silica-coated magnetite were prepared using the sol−immobilization method. The silica-coated magnetite support (FFSi) was prepared by reverse microemulsion and functionalized with amino groups ($FFSiNH_2$), as previously reported.[34]

The immobilization of the preformed Ni_xPd_y nanoparticles on the magnetic support was carried out in a Schlenk flask under an argon atmosphere. To 1 g of $FFSiNH_2$ previously dried under vacuum for 1 h (0.2 mbar, r.t.) was added 6 mL of the nonpurified solution of Ni_xPd_y nanoparticles described above. The mixture was stirred for 2 h, the solid was magnetically recovered, and the final solution was removed with a syringe. The solid was washed four times with 6 mL of pentane and then dried under vacuum conditions for 1 h (0.2 mbar, r.t.). The final nanomaterials, denoted as $FFSiNH_2Ni_xPd_y$, were stored under air conditions.

2.5. Catalytic Tests. The catalytic tests were based on the hydrogenation of cyclohexene under solvent-free conditions. The cyclohexene was dried with $MgSO_4$ and distilled under N_2 just before its use. All transfers were performed in an N_2 atmosphere with a syringe. The catalytic reactions were carried out in a Fischer−Porter reactor connected to a hydrogen gas reservoir by a pressure regulator responsible for keeping a constant pressure inside the reactor. The hydrogen consumption was measured with a signal transducer connected to the hydrogen reservoir. The catalytic activity of each catalyst was determined at the beginning of the reaction by the slope of the linear curve obtained from the plot of TON (turnover number) versus the time of the reaction. In a typical experiment, an amount of catalyst containing 9.75×10^{-4} mmol of metal (nickel and palladium) was first submitted to a 1 bar manometric of hydrogen and 75 °C for 1 h for the catalyst activation. Fresh distilled cyclohexene (1.6 g, 19.5 mmol) was then added, and the mixture, under magnetic stirring, was

dx.doi.org/10.1021/cs500337a | ACS Catal. 2014, 4, 1735−1742

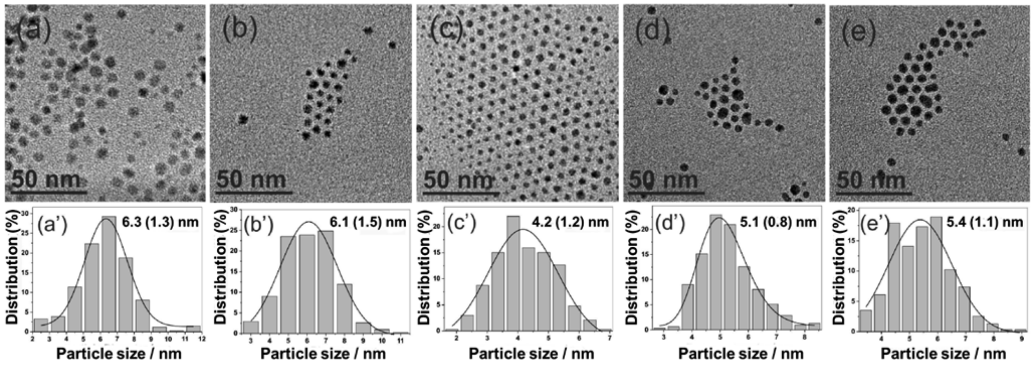

Figure 1. Electron micrographs of (a) Ni, (b) Ni_9Pd, (c) NiPd, (d) $NiPd_9$, and (e) Pd colloidal nanoparticles obtained at 110 °C in toluene, in the presence of HDA (metal/HDA = 1:10), and the corresponding size histograms (a′), (b′), (c′), (d′), and (e′), respectively.

submitted to a 6 bar manometric of dihydrogen, and heated at 75 °C until the completion of the reaction.

2.6. Characterization Techniques. The morphology, size, and dispersion of colloidal and supported bimetallic nanoparticles were characterized by an electronic microscopy technique using a JEOL JEM 2010 microscope, working at 200 kV with a resolution of 2.35 Å. The samples were prepared by the deposition of a drop of the suspension on a covered holey copper grid, followed by drying under vacuum conditions over 15 h. The diameter of ca. 200 particles was measured for each sample from enlarged micrographs using Image Tool software. Using Origin software, size-distribution histograms fitted to Gaussian or LogNormal functions were used to determine the mean diameters and the statistical size distributions of the nanoparticles.

The Ni and Pd content was measured using an inductively coupled plasma optical emission spectrometer (ICP OES) at the "Service Central d' Analyses" of the National Center for Scientific Research (CNRS) in Lyon using an iCAP 6300 from Thermo Scientific, and at the "Central Analítica" of the Institute of Chemistry at the University of São Paulo (IQ/USP) using the Spectro Ciros CCD. The CHN measurements were carried out with a PERKIN ELMER 2400 series II at the "Service d' Analyses" of LCC CNRS-Toulouse.

The magnetization curves of the nanocatalysts were acquired on a Quantum Design Model MPMS 5.5 SQUID magnetometer (5 T, at 2K). The analysis was performed by the service of magnetic measurements of CNRS-Toulouse. The saturation magnetization was deduced from the nickel and palladium content determined ICP OES analysis.

The dispersion of metal atoms within the individual nanoparticles was investigated by the acquisition of compositional maps using a JEOL-JEM 2100F microscope available at the Nanotechnology National Laboratory (LNNano) (CNPEM, Campinas, SP). The XED-Spectrum Imaging technique was employed with a Digital Micrograph 1.8 system (Gatan, Inc.) controlling a Thermo-Noran XEDS. The spectrum images (SI) were acquired with a dwell time of 2 s/pixel using the drift correction facility at every 100 s. XED spectra were acquired in the 0−10 keV energy range at each pixel. Electron probe sizes of ca. 0.7 nm were obtained operating the JEM 2100F instrument in the STEM mode, allowing enough current density at each sample point for the acquisition of statistically significant X-ray counts for the investigated elements.

The X-ray photoelectron spectroscopy analysis was carried out with a spherical analyzer VSWHA-100 equipped with an aluminum anode (Al line Kα, hν = 1486.6 eV). The spectra were corrected for sample charging by adjusting the binding energy for Si 2p in SiO_2 to 103.5 eV. The data was processed by removing a Shirley background and fitting Gaussian curves.

For the catalytic tests, the completion of the hydrogenation reactions was checked carefully by determining the end of hydrogen consumption, and by gas chromatography, using a Shimadzu GC-2010 with a 30 m Rtx-5 column. Parameters: Ti = 50 °C, Tf = 150 °C, heating rate = 10 °C/min.

3. RESULTS AND DISCUSSION

3.1. Preparation of Ni_xPd_y Nanoparticles. The preparation of the monometallic nanoparticles by the decomposition of $Ni(cod)_2$[35] or $Pd_2(dba)_3$[36] in a tetrahydrofuran solution under dihydrogen and in the presence of hexadecylamine (HDA) has been previously reported. Well-defined palladium and nickel nanoparticles were obtained with a metal/HDA molar ratio of 1:10. However, different morphologies were observed according to the temperature of decomposition of the corresponding organometallic precursors (nickel nanorods at 70 °C[35] and spherical palladium nanoparticles at r.t.[36]). The decomposition of $Ni(cod)_2$ in the presence of HDA requires a higher temperature than $Pd_2(dba)_3$ to produce metal nanoparticles, due to a slower rate of decomposition.

In this study, we first reinvestigated the synthesis of monometallic nickel and palladium nanoparticles with the aim to find adequate conditions to obtain nanoparticles of similar size and morphology. In order to reach higher reaction temperatures to perform the decomposition of the organometallic precursors, we replaced tetrahydrofuran with toluene. Moreover, toluene is a noncoordinating solvent, whereas tetrahydrofuran may interact with the metal surface. Size-controlled nanoparticles were thus synthesized in toluene under 3 bar of dihydrogen at 110 °C, at a 1:10 metal/HDA molar ratio. The same reaction conditions were applied to prepare bimetallic nickel−palladium nanoparticles by codecomposition of the two organometallic precursors. Figure 1a−e show typical electron micrographs of the resulting nearly spherical Ni, Ni_9Pd, NiPd, $NiPd_9$, and Pd nanoparticles, with mean diameters of 6.3(1.3), 6.1(1.5), 4.2(1.2), 5.1(0.8), and 5.4(1.1) nm, respectively.

The degree of purification of the nanoparticles is important for many applications; however, we met some difficulties in removing the nanoparticles from the organic media containing excess HDA. The strategy followed in this study was repeated cycles of precipitation of the nanoparticles, with cold pentane in an ice bath, but it was not possible to avoid the simultaneous

dx.doi.org/10.1021/cs500337a | ACS Catal. 2014, 4, 1735−1742

precipitation of HDA, resulting in low metal content in each isolated powder (determined by ICP OES, Table 1). The Ni/Pd ratio determined experimentally was very close to the theoretical ratio, which suggests a good control on the decomposition of both metal precursors. Conversely, the purification performed at room temperature (entry 7, Table 1) greatly improved the removal of HDA, but the large amount of wasted nanoparticles made this process impractical. We will later show that the preparation of the supported nanomaterials by the sol–immobilization method could be carried out with nonpurified colloidal solutions, which avoids the purification steps.

Table 1. Composition of Monometallic and Bimetallic Nanoparticle Powders

entry	sample	Ni (wt %)	Pd (wt %)	Ni/Pd (mol/mol)
1	Ni	4.75		1:0
2	Ni_9Pd	2.34	0.43	9.1:0.9
3	NiPd	1.32	2.31	5.1:4.9
4	$NiPd_9$	0.28	3.91	1.1:8.9
6	Pd		16.25	0:1
7[a]	Pd		85	0:1

[a]Purified at room temperature.

3.2. Preparation of Supported Ni_xPd_y Catalysts. For this study, we have chosen a catalyst support that exhibits superparamagnetic properties, and therefore, it can be recovered with a permanent magnet (high saturation magnetization), and can be redispersed immediately after removal of the magnetic field (absence of remanence). The magnetic separation is a powerful tool for easy and fast separation of the catalyst from liquid phase reactions, avoiding laborious work-up procedures for catalyst separation and product purification, and the exposure of the catalyst to air. Magnetically recoverable catalysts have been used in a wide range of catalytic reactions to develop more efficient and green chemical processes.[37−39]

The process to prepare the magnetically recoverable catalysts consists of adding colloidal suspensions of Ni, Ni_9Pd, NiPd, $NiPd_9$, and Pd nanoparticles to a magnetic solid composed of silica-coated magnetite nanoparticles for impregnation. However, the immobilization of metal nanoparticles into the magnetic support is not straightforward, and it depends on the strength of the metal nanoparticle-to-support interactions. We have previously reported that the functionalization of the support surfaces can enhance the impregnation rate of metal salts[40] and metal nanoparticles[41] on silica-based supports, an important step for catalyst preparation. The functionalization of solid supports has become a strategy to prepare supported homogeneous catalysts[42,43] and nanocatalysts.[44] In this study, we first observed that the loading of metal in the chosen magnetic support, FFSi, was very low (0.24 wt %), but if the magnetic support was functionalized with the amine group, $FFSiNH_2$, then the metal loading was enhanced to 0.80 wt %. Therefore, only $FFSiNH_2$ was further used as support. The nanomaterials obtained after the metal nanoparticle immobilization are denoted as $FFSiNH_2Ni$, $FFSiNH_2Ni_9Pd$, $FFSiNH_2NiPd$, $FFSiNH_2NiPd_9$, and $FFSiNH_2Pd$. The TEM images of the supported nanocatalysts depicted in Figure 2 confirm the core–shell structure of the support material, as previously reported,[34] and the metal nanoparticles immobilized on the silica surface.

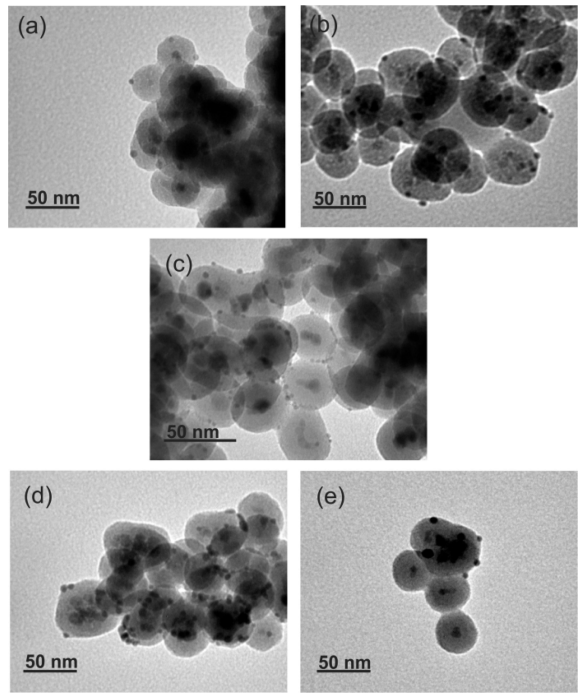

Figure 2. Electron micrographs of the supported colloidal nickel–palladium nanoparticles. (a) $FFSiNH_2Ni$, (b) $FFSiNH_2Ni_9Pd$, (c) $FFSiNH_2NiPd$, (d) $FFSiNH_2NiPd_9$, and (e) $FFSiNH_2Pd$.

It is worth mentioning that the supported Ni_xPd_y nanoparticles had the excess HDA removed during a post-impregnation washing step, which consists of a repeated solvent extraction procedure with pentane. This was confirmed by the low carbon contents of the supported nanocatalysts, determined by C/H/N analysis (Table 2). Additionally, the C/H/N results are very close to the values obtained for the support without nanoparticles. Approximately 30% of the theoretical amount of metal was deposited in the amine-functionalized support, and the Ni/Pd ratio remained the same after immobilization (Table 2).

3.3. Characterization of the Bimetallic Nickel–Palladium System. The synthesis and characterization of bimetallic nanoparticles are complicated because different metal domain distribution are possible, such as core–shell structures, ordered or disordered nanoalloys, and a mixture of the two metals as monometallic nanoparticles. The information concerning the metal domain distribution is crucial to understand the catalytic behavior of bimetallic nanoparticles. The magnetic properties of the nickel–palladium nanoparticles were studied before immobilization to avoid the overlap with the magnetic properties of the magnetic support. In Figure 3, the obtained magnetization curve $M \times H$ showed that the air-protected samples Ni, Ni_9Pd, NiPd, and $NiPd_9$ exhibit saturation magnetization of 51, 32, 30, and 10.8 emu·g^{-1}, respectively. The values obtained for Ni, NiPd, and $NiPd_9$ are in agreement with bulk nickel and nickel–palladium alloys under similar analysis conditions and similar Ni/Pd ratio (see refs 35, 45, and 46 for Ni, ref 47 for NiPd, and refs 48 and 49 for $NiPd_9$). We could not find information about Ni_9Pd alloys under the same analysis conditions. The saturation magnetization values obtained are consistent with the presence of both metals in the same nanoparticle, which suggests the formation of nanoalloys.

dx.doi.org/10.1021/cs500337a | ACS Catal. 2014, 4, 1735−1742

Table 2. Elemental Analysis Determined for Supported Bimetallic Ni_xPd_y Nanoparticles

entry	sample	Ni (%)	Pd (%)	Ni/Pd (mol/mol)	C (%)	H (%)	N (%)
1	$FFSiNH_2Ni$	0.64		1:0	4.53	0.97	0.93
2	$FFSiNH_2Ni_9Pd$	0.36	0.05	9.3:0.7	2.94	1.64	0.77
3	$FFSiNH_2NiPd$	0.43	0.63	5.1:4.9	3.83	0.96	0.96
4	$FFSiNH_2NiPd_9$	0.05	0.68	1.1:8.9	3.35	1.62	0.96
5	$FFSiNH_2Pd$		0.8	0:1	3.99	1.12	0.93
6	$FFSiNH_2$				3.02	0.81	0.58

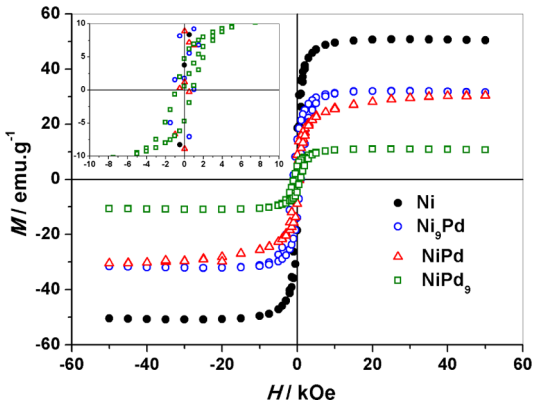

Figure 3. Magnetization curve $M \times H$ of Ni, Ni_9Pd, NiPd, and $NiPd_9$ colloidal nanoparticles at 2K.

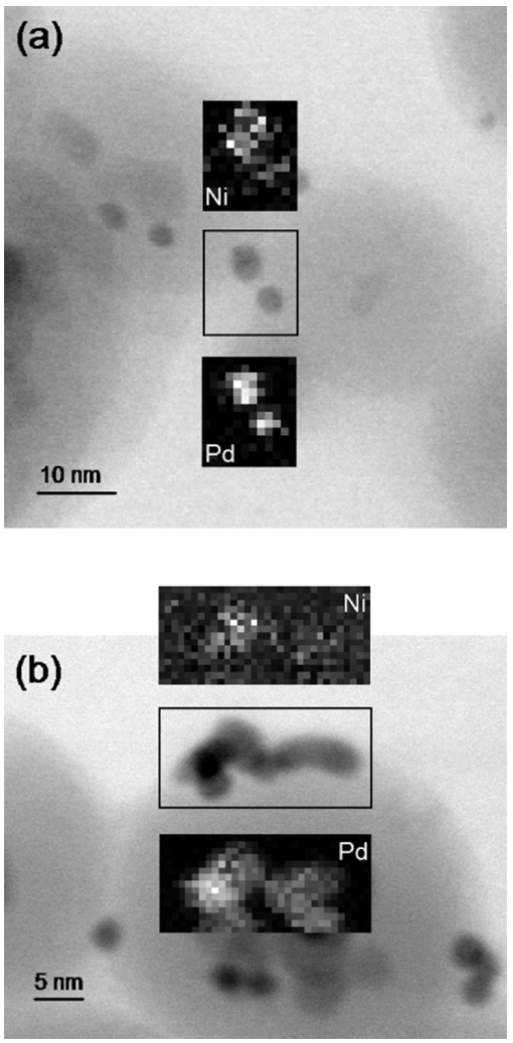

Figure 4. Bright-field STEM images and the corresponding nickel and palladium compositional maps of representative regions of (a) $FFSiNH_2NiPd$ and (b) $FFSiNH_2NiPd_9$.

The metal domain distributions on the supported Ni_xPd_y nanoparticles were assessed from chemical mapping using the STEM-XEDS technique as presented in Figure 4. As shown in the respective compositional maps, there is some segregation of nickel at the nanoparticle surface. This observation is consistent with the analysis of many compositional maps, obtained from different regions of the samples.

XPS analysis (Figure 5a and Table 3) showed that the nickel on the surface of the bimetallic nanoparticles is present mostly in its oxidized form. The intensity of the satellite peaks at around 861 eV for $FFSiNH_2Ni$, $FFSiNH_2Ni_9Pd$, and $FFSiNH_2NiPd$ is in agreement with the presence of oxidized nickel (Figure 5a).[50] The 2p3/2 peaks for the samples $FFSiNH_2NiPd$, $FFSiNH_2NiPd_9$ are shifted toward the binding energy of Ni(0) species,[51] probably because the higher amount of Ni−Pd bonds in these systems compared to $FFSiNH_2Ni_9Pd$. The binding energies of Pd 3d5/2 and 3d3/2 and the difference between them (5 eV) are consistent with Pd(0)[50] in the samples $FFSiNH_2Pd$, $FFSiNH_2NiPd_9$ and $FFSiNH_2NiPd$. As observed in Figure 5(b), there is a small shift of the Pd 3d3/2 peaks to lower binding energies for the bimetallic catalysts compared to pure Pd system, which is in agreement with the observed for others NiPd alloy.[52] The binding energy for Pd 3d in the sample $FFSiNH_2Ni_9Pd$ was not determined because of the low Pd content.

The presence of segregated regions of Pd and Ni in the bimetallic nanoparticles observed by STEM-XEDS in this study is common in nickel−palladium alloys because of the mismatch of the atomic size of Ni and Pd, which favors the formation of a disordered alloy system.[53] The accumulation of nickel on the nanoparticle surface provides some evidence about the mechanism of the formation of the bimetallic nanoparticles from the organometallic precursors, $Ni(cod)_2$ and $Pd_2(dba)_3$. From previous results,[35,36] it was shown that the reactivity of $Pd_2(dba)_3$ and $Ni(cod)_2$ with dihydrogen is quite different. Under the studied conditions, it is expected that $Pd_2(dba)_3$ decomposes first into Pd(0) nanoparticles, which may then catalyze the decomposition of $Ni(cod)_2$, leading to bimetallic systems containing palladium at the core and excess nickel on the surface. Additionally, the characterization by STEM-EDS and XPS could be only performed after air exposure, which could cause nickel oxidation and the reorganization of the nanoparticles structure accumulating nickel oxide on the nanoparticle surface.

3.4. Catalytic Activity of Nickel−Palladium Nanocatalysts in the Hydrogenation of Cyclohexene. The bimetallic nanocatalysts were applied in the hydrogenation of cyclohexene, a model substrate for the hydrogenation of olefins.[54−56] The reaction was monitored by hydrogen

dx.doi.org/10.1021/cs500337a | ACS Catal. 2014, 4, 1735−1742

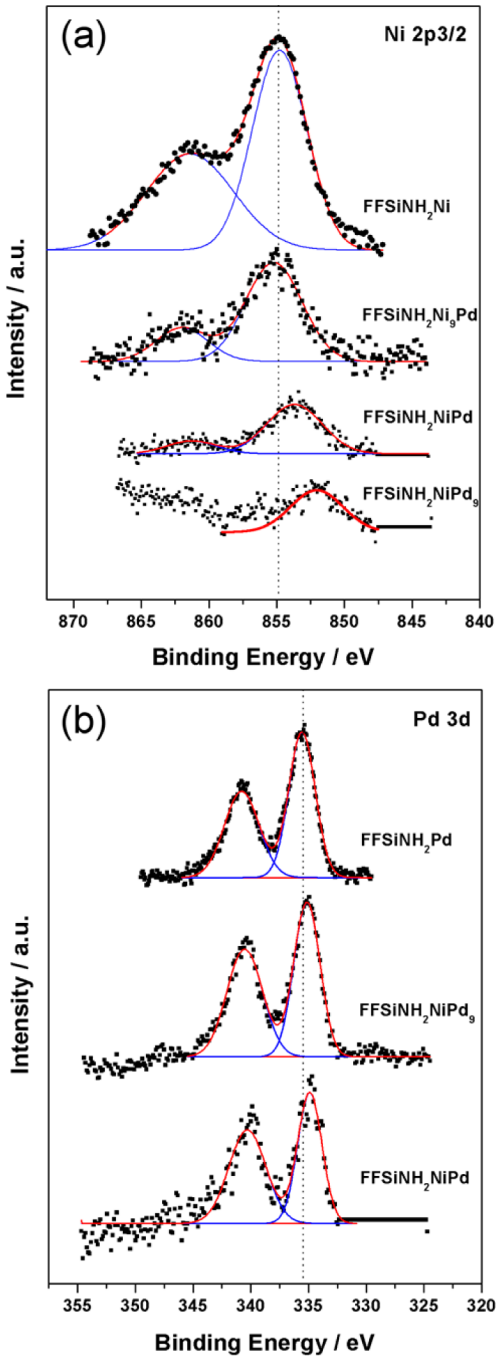

Figure 5. XPS spectra of the supported Ni_xPd_y, Ni and Pd nanoparticles. (a) Ni 2p 3/2 and (b) Pd 3d.

Table 3. XPS Parameters for Supported Bimetallic Ni_xPd_y Nanoparticles

		BE (eV)	
entry	sample	$Ni_{2p3/2}$	$Pd_{3d5/2;3/2}$
1	$FFSiNH_2Ni$	854.8	
2	$FFSiNH_2Ni_9Pd$	854.7	ND[a]
3	$FFSiNH_2NiPd$	853.7	340.3; 334.9
4	$FFSiNH_2NiPd_9$	852.1	340.5; 335.7
5	$FFSiNH_2Pd$		340.7; 335.5

[a]ND = not detected.

consumption versus time, and the turnover frequency (TOF) was expressed by $mol_{cyclohexene} \cdot mol_{Ni+Pd}^{-1} \cdot h^{-1}$ at initial rates.

The catalytic activities obtained for the monometallic nickel and palladium and the series of bimetallic nanomaterials in the hydrogenation of cyclohexene are summarized in Table 4.

Table 4. Catalytic Performance of $FFSiNH_2Ni_xPd_y$ in the Hydrogenation of Cyclohexene[a]

entry	catalyst	TOF[b]	time[c] (min)
1	$FFSiNH_2Ni$	0	nr
2	$FFSiNH_2Ni_9Pd$	0	nr
3	$FFSiNH_2NiPd$	14 000	150
4	$FFSiNH_2NiPd_9$	56 000	25
5	$FFSiNH_2Pd$	37 000	45
6	$NiPd_9$	15 900	150

[a]Reaction conditions: 20 000 mol of cyclohexene per mol of metal, 6 bar of H_2, 75 °C. [b]TOF expressed as $mol_{cyclohexene} \cdot mol_{Ni+Pd}^{-1} \cdot h^{-1}$. [c]Time for complete reaction. nr = no reaction after 12 h.

Usually, nickel is less active than palladium in hydrogenation reactions;[57] therefore, we could expect that nickel's segregation to the surface of the bimetallic catalysts would result in less active catalysts than the monometallic palladium catalyst. The $FFSiNH_2NiPd$ and $FFSiNH_2Ni_9Pd$ catalysts were indeed less active than the monometallic $FFSiNH_2Pd$, but the $FFSiNH_2NiPd_9$ catalyst was unexpectedly more active than the monometallic one. Because the sizes of the nanoparticles in $FFSiNH_2Pd$ and $FFSiNH_2NiPd_9$ are very close (ca. 5.4 and 5.1 nm, respectively), we can exclude a size effect, and the catalytic results can be due to a synergistic effect of nickel and palladium.

In hydrogenation reactions, the enhancement of catalytic activity for the bimetallic nickel–palladium catalysts (bulk and nanoparticle systems), compared with the monometallic palladium catalyst, is usually explained by the segregation of palladium on the alloy surface.[58] The improvement of the palladium activity when deposited on the nickel surface was discussed, by theoretical and experimental studies, in terms of the influence of nickel on the electronic properties of palladium (even for palladium coverage higher than 1 atomic layer),[59−62] or in terms of the partial relaxation of the palladium strain that creates new active sites.[63,64]

Changes in the electronic properties of palladium usually occur when bimetallic systems are formed with a more electronegative metal than palladium,[65] which is not the case of nickel. However, the magnetic properties of nickel must also be considered as causing electronic modifications to palladium in nickel–palladium systems. For example, theoretical studies show that nickel promotes an enhancement of the magnetic moment of palladium in a bimetallic system.[66] In this study, the characterization techniques used suggest that nickel is segregated on the surface of the bimetallic nanoparticles, and the most active catalyst contains low nickel loading (1:9 Ni/Pd molar ratio). It is more reasonable to expect that the relaxation of the interlayer and intralayer distances caused by the geometric arrangement of the atoms, as observed for nickel ultrathin films deposited on palladium,[67] contributes to the increased activity of this bimetallic nanocatalyst, outperforming the Pd monometallic catalyst. However, it is important to consider that the surface chemistry in nanoparticles is different from the bulk counterparts, and other undetermined effects can probably be related to the observed catalytic activity.

dx.doi.org/10.1021/cs500337a | ACS Catal. 2014, 4, 1735−1742

The nonsupported colloidal nanoparticles, $NiPd_9$, do not exhibit the same catalytic activity as the $FFSiNH_2NiPd_9$ supported catalyst under similar reaction conditions (see Table 4, entry 6). This difference can be related to the decrease in the HDA coverage at the metal surface, after the removal of the HDA during the washing steps, which is facilitated by the immobilization of the colloidal nanoparticles on the silica support. Additionally, when the amino functionalized support ($FFSiNH_2$) is added to the solution containing HDA-stabilized nanoparticles, the $-NH_2$ groups grafted on the support can enhance the metal−support interaction, which results in the attachment of the nanoparticles onto the surface of the solid. Partial displacement of the HDA by those ligands grafted on the support surface is expected, and the new nanoparticle−support interactions can also affect the catalytic properties of the supported metal nanoparticles.

There are a few examples of similar studies concerning the hydrogenation of olefins using nickel−palladium nanocatalysts. Massard et al.[68] prepared core(Ni)−shell(Pd) nanoparticles supported on α-alumina using two methods: (1) mixing alumina-supported Ni(0) nanoparticles into a solution of palladium acetylacetonate in the presence of dihydrogen and (2) synthesizing colloidal nanoparticles by the sequential reduction of nickel and palladium acetylacetonate, followed by impregnation on an alumina support. These catalysts, with size diameters of 5−6 nm, were tested in the selective hydrogenation of buta-1,3-diene, but the TOF of the bimetallic systems was 10 times lower than that of monometallic palladium catalysts. The authors concluded that the surface reconstruction during catalysis, which could be considered responsible for the enhancement of the catalytic activity of the palladium on the nickel surface, did not occur on the 5 nm supported nickel−palladium particles. However, in our study, we observed a different behavior: a small amount of Ni concentrated on the surface of 5 nm nickel−palladium nanoparticles can promote the catalytic activity of palladium.

3.4. Recycling Experiments. A great advantage of using a magnetic support in catalysis relies on the possibility of easily separating the catalyst from the products by simply applying an external magnet. Recycling experiments were carried out for the most active $FFSiNH_2NiPd_9$ catalyst in the hydrogenation of cyclohexene. The catalytic reactions during the recycling experiments were performed until completion, and the initial TOFs were obtained from the slope of the hydrogenation curves (turnover number versus time) at low conversion (<20% conversion). The catalyst exhibited high stability upon recycling, and after five cycles, no significant decrease in activity was observed, compared to the initial catalytic performance (Figure 6). The amount of palladium and nickel in the cyclohexane product was quantified by ICP-OES (palladium <0.02 ppm and nickel <0.01 ppm), and no leaching was observed. The functionalization of the magnetic support with amino groups not only contributed to improve the loading of the metal nanoparticles but also promoted a strong interaction of the metal nanoparticles and the support surface, thus avoiding metal leaching.[44]

4. CONCLUSION

We reported in this study, for the first time, the preparation of nickel−palladium nanoparticles through the codecomposition of $Pd_2(dba)_3$ and $Ni(cod)_2$ organometallic precursors. The synthesis of colloidal nickel−palladium nanoparticles in the presence of 10 mol equiv of HDA allowed the formation of well-controlled bimetallic nanoparticles with similar size and morphology in all Ni/Pd molar ratio studied. We then investigated the sol−immobilization method for the preparation of supported bimetallic nickel−palladium using an amino-functionalized silica-coated magnetite support. The excess HDA was easily removed after the immobilization of the colloidal bimetallic nanoparticles on the magnetic support by pentane washing. The supported catalysts were very active for cyclohexene hydrogenation. The most active nanocatalyst contained the 1:9 Ni/Pd molar ratio, which is economically important, because it provides a catalyst with less Pd but more activity than the Pd monometallic counterpart. The magnetic separation was crucial to the performance of the catalysts presented in this study, because it provides excellent separation of the catalyst from the liquid products without metal leaching and exposure to air, allowing for efficient recycling. Further studies will be performed to investigate the possibility of synthesizing NiPd nanoparticles with good size control and dispersion by direct decomposition of the organometallic precursors over the support, as already demonstrated for Ni and Pd monometallic nanoparticles.[32,33]

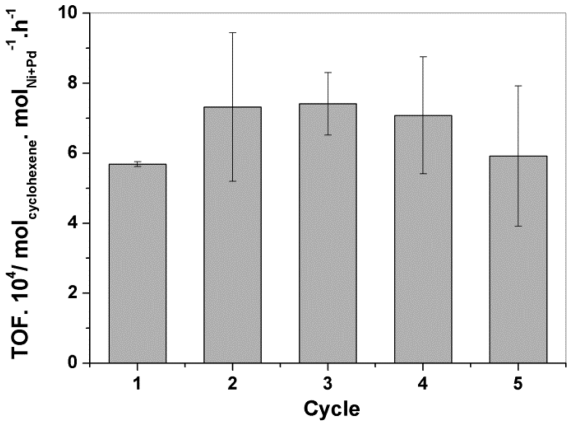

Figure 6. Successive cyclohexene hydrogenation reactions using $FFSiNH_2NiPd_9$.

AUTHOR INFORMATION

Corresponding Authors

*(L.M.R.) E-mail: lrossi@iq.usp.br.

*(K.P.) E-mail: Karine.Philippot@lcc-toulouse.fr.

Notes

The authors declare no competing financial interest.

ACKNOWLEDGMENTS

The authors would like to thank the Brazilian agencies FAPESP, CAPES, and CNPq for their financial support. The support received from the International Cooperation Program CAPES-COFECUB (grant 695/10) and CNRS is also appreciated. Additionally, LNNano-CNPEM (Campinas, Brazil) and TEMSCAN-UPS (Toulouse, France) are acknowledged for the use of their TEM/HRTEM facilities. The authors would like to thank Dr. Renato F. Jardim and Dr. Sueli H. Masunaga (Instituto de Física—Universidade de São Paulo) for discussions on magnetic measurement data.

REFERENCES

(1) Richards, R.; Koodali, R.; Klabunde, K.; Erickson, L. *Nanoscale Materials in Chemistry: Environmental Application*; ACS Publications: Washington DC, 2011.

(2) Schmid, G. *Nanoparticles: From Theory to Application*, 2nd ed., Wiley-VCH: Weinheim, 2012.
(3) Yamamoto, T. A.; Kageyama, S.; Seino, S.; Nitani, H.; Nakagawa, T.; Horioka, R.; Honda, Y.; Ueno, K.; Daimon, H. *Appl. Catal., A* **2011**, *396*, 68−75.
(4) Wei, Y.-C.; Liu, C.-W.; Chang, W.-J.; Wang, K.-W. *J. Alloys Compd.* **2011**, *509*, 535−541.
(5) Somorjai, G. A.; Frei, H.; Park, J. Y. *J. Am. Chem. Soc.* **2009**, *131*, 16589−16605.
(6) Philippot, K.; Serp, P. *Concepts in Nanocatalysis*; Wiley-VCH: Weinheim, 2013.
(7) Liu, M.; Zhang, J.; Liu, J.; Yu, W. W. *J. Catal.* **2011**, *278*, 1−7.
(8) Jeon, T.-Y.; Lee, K.-S.; Yoo, S. J.; Cho, Y.-H.; Kang, S. H.; Sung, Y.-E. *Langmuir* **2010**, *26*, 9123−9129.
(9) Chen, T.-Y.; Lin, T.-L.; Luo, T.-J. M.; Choi, Y.; Lee, J.-F. *ChemPhysChem* **2010**, *11*, 2383−2392.
(10) Chen, C.-H.; Sarma, L. S.; Wang, D.-Y.; Lai, F.-J.; Al Andra, C.-C.; Chang, S.-H.; Liu, D.-G.; Chen, C.-C.; Lee, J.-F.; Hwang, B.-J. *ChemCatChem.* **2010**, *2*, 159−166.
(11) Murthy, A.; Manthiram, A. *Electrochem. Commun.* **2011**, *13*, 310−313.
(12) Wang, D.; Li, Y. *Adv. Mater.* **2011**, *23*, 1044−1060.
(13) Li, C.; Shao, Z.; Pang, M.; Williams, C. T.; Zhang, X.; Liang, C. *Ind. Eng. Chem. Res.* **2012**, *51*, 4934−4941.
(14) Dehm, N. A.; Zhang, X.; Buriak, J. M. *Inorg. Chem.* **2010**, *49*, 2706−2714.
(15) Arakawa, T.; Seki, H.; Ohshima, M.-a.; Kurokawa, H.; Miura, H. *Bull. Chem. Soc. Jpn.* **2009**, *82*, 627−629.
(16) Astruc, D. *Nanoparticles and Catalysis*; Wiley-VCH: Weinheim, 2008.
(17) Roucoux, A.; Schulz, J.; Patin, H. *Chem. Rev.* **2002**, *102*, 3757−3778.
(18) Sanchez-Dominguez, M.; Pemartin, K.; Boutonnet, M. *Curr. Opin. Colloid Interface Sci.* **2012**, *17*, 297−305.
(19) Liu, X. W.; Wang, D. S.; Li, Y. D. *Nano Today* **2012**, *7*, 448−466.
(20) Kalidindi, S. B.; Sanyal, U.; Jagirdar, B. R. *ChemSusChem* **2011**, *4*, 317−324.
(21) Phillipot, K.; Chaudret, B. In *Comprehensive Organometallic Chemistry III*; Crabtree, R. H., Mingos, M. P., Eds.; Elsevier: Amsterdam, 2007; p 71.
(22) Lara, P.; Philippot, K.; Chaudret, B. *ChemCatChem.* **2013**, *5*, 28−45.
(23) Kinayyigit, S.; Lara, P.; Lecante, P.; Philippot, K.; Chaudret, B. *Nanoscale* **2014**, *6*, 539−546.
(24) Matsura, V.; Guari, Y.; Reye, C.; Corriu, R. J. P.; Tristany, M.; Jansat, S.; Philippot, K.; Maisonnat, A.; Chaudret, B. *Adv. Funct. Mater.* **2009**, *19*, 3781−3787.
(25) Garcia-Suarez, E. J.; Tristany, M.; Garcia, A. B.; Colliere, V.; Philippot, K. *Microporous Mesoporous Mater.* **2012**, *153*, 155−162.
(26) Chaudret, B.; Philippot, K. *Oil Gas Sci. Technol.* **2007**, *62*, 799−817.
(27) Castillejos, E.; Debouttiere, P.-J.; Roiban, L.; Solhy, A.; Martinez, V.; Kihn, Y.; Ersen, O.; Philippot, K.; Chaudret, B.; Serp, P. *Angew. Chem., Int. Ed.* **2009**, *48*, 2529−2533.
(28) Gates, B. C. *Chem. Rev.* **1995**, *95*, 511−522.
(29) Davis, S. E.; Ide, M. S.; Davis, R. J. *Green Chem.* **2013**, *15*, 17−45.
(30) Campelo, J. M.; Luna, D.; Luque, R.; Marinas, J. M.; Romero, A. A. *ChemSusChem* **2009**, *2*, 18−45.
(31) Garcia-Suarez, E. J.; Balu, A. M.; Tristany, M.; Garcia, A. B.; Philippot, K.; Luque, R. *Green Chem.* **2012**, *14*, 1434−1439.
(32) Costa, N. J. S.; Jardim, R. F.; Masunaga, S. H.; Zanchet, D.; Landers, R.; Rossi, L. M. *ACS Catal.* **2012**, *2*, 925−929.
(33) Guerrero, M.; Costa, N. J. S.; Vono, L. L. R.; Rossi, L. M.; Gusevskaya, E. V.; Philippot, K. *J. Mater. Chem. A* **2013**, *1*, 1441−1449.
(34) Jacinto, M. J.; Kiyohara, P. K.; Masunaga, S. H.; Jardim, R. F.; Rossi, L. M. *Appl. Catal. A-Gen.* **2008**, *338*, 52−57.
(35) Cordente, N.; Respaud, M.; Senocq, F.; Casanove, M. J.; Amiens, C.; Chaudret, B. *Nano Lett.* **2001**, *1*, 565−568.
(36) Ramirez, E.; Jansat, S.; Philippot, K.; Lecante, P.; Gomez, M.; Masdeu-Bulto, A. M.; Chaudret, B. *J. Organomet. Chem.* **2004**, *689*, 4601−4610.
(37) Shylesh, S.; Schuenemann, V.; Thiel, W. R. *Angew. Chem., Int. Ed.* **2010**, *49*, 3428−3459.
(38) Rossi, L. M.; Garcia, M. A. S.; Vono, L. L. R. *J. Brazil. Chem. Soc.* **2012**, *23*, 1959−1971.
(39) Polshettiwar, V.; Luque, R.; Fihri, A.; Zhu, H.; Bouhrara, M.; Bassett, J.-M. *Chem. Rev.* **2011**, *111*, 3036−3075.
(40) Jacinto, M. J.; Silva, F. P.; Kiyohara, P. K.; Landers, R.; Rossi, L. M. *ChemCatChem.* **2012**, *4*, 698−703.
(41) Oliveira, R. L.; Zanchet, D.; Kiyohara, P. K.; Rossi, L. M. *Chem.—Eur. J.* **2011**, *17*, 4626−4631.
(42) Neves, A. C. B.; Calvete, M. J. F.; Pinho e Melo, T. M. V. D.; Pereira, M. M. *Eur. J. Org. Chem.* **2012**, *2012*, 6309−6320.
(43) Collis, A. E. C.; Horvath, I. T. *Catal. Sci. Technol.* **2011**, *1*, 912−919.
(44) Costa, N. J. S.; Rossi, L. M. *Nanoscale* **2012**, *4*, 5826−5834.
(45) Chen, Y.; Peng, D.-L.; Lin, D.; Luo, X. *Nanotechnology* **2007**, *18*, 505703.
(46) Cullity, B. D.; Graham, C. D. *Introduction to Magnetic Materials*, 2nd ed,; John Wiley & Son: Hoboken, NJ, 2009.
(47) Fischer, G.; Herr, A.; Meyer, A. J. P. *J. Appl. Phys.* **1968**, *39*, 545−546.
(48) Chouteau, G.; Fourneau, R.; Gobrecht, K.; Tournier, R. *Phys. Rev. Lett.* **1968**, *20*, 193−195.
(49) Crangle, J.; Scott, W. R. *J. Appl. Phys.* **1965**, *36*, 921−927.
(50) Moulder, J. F.; Stickle, W. F.; Sobol, P. E.; Bomben, K. D. *Handbook of X-ray Photoelectron Spectroscopy Physical Electronics*; Perkin-Elmer Corporation Physical Electronics Division: Eden Prairie, Minnesota, 1979; p 80, 110.
(51) Damyanova, S.; Pawelec, B.; Arishtirova, K.; Fierro, J. L. G. *Int. J. Hydrogen Energy* **2011**, *36*, 10635−10647.
(52) Li, R.; Wei, Z.; Huang, T.; Yu, A. *Electrochim. Acta* **2011**, *56*, 6860−6865.
(53) Wang, L. G.; Zunger, A. *Phys. Rev. B* **2003**, *67*, 092103.
(54) Watzky, M. A.; Finke, R. G. *J. Am. Chem. Soc.* **1997**, *119*, 10382−10400.
(55) Besson, C.; Finney, E. E.; Finke, R. G. *J. Am. Chem. Soc.* **2005**, *127*, 8179−8184.
(56) Besson, C.; Finney, E. E.; Finke, R. G. *Chem. Mater.* **2005**, *17*, 4925−4938.
(57) Moulijn, J. A.; van Leeuwn, P. W. N. M.; van Santen, R. A. *Catalysis: An Integrated Approach to Homogeneous, Heterogeneous and Industrial Catalysis*; Elsevier: Amsterdam, 1993.
(58) Batirev, I. G.; Leiro, J. A. *J. Electron Spectrosc.* **1995**, *71*, 79−86.
(59) Hermann, P.; Tardy, B.; Simon, D.; Guigner, J. M.; Bigot, B.; Bertolini, J. C. *Surf. Sci.* **1994**, *307*, 422−427.
(60) Hermann, P.; Simon, D.; Sautet, P.; Bigot, B. *J. Catal.* **1997**, *167*, 33−42.
(61) Hermann, P.; Guigner, J. M.; Tardy, B.; Jugnet, Y.; Simon, D.; Bertolini, J. C. *J. Catal.* **1996**, *163*, 169−175.
(62) Bertolini, J. C.; Miegge, P.; Hermann, P.; Rousset, J. L.; Tardy, B. *Surf. Sci.* **1995**, *331*, 651−658.
(63) Filhol, J. S.; Simon, D.; Sautet, P. *Surf. Sci.* **2001**, *472*, L139−L144.
(64) Filhol, J. S.; Saint-Lager, M. C.; De Santis, M.; Dolle, P.; Simon, D.; Baudoing-Savois, R.; Bertolini, J. C.; Sautet, P. *Phys. Rev. Lett.* **2002**, *89*, 146106.
(65) Knecht, M. R.; Pacardo, D. B. *Anal. Bioanal. Chem.* **2010**, *397*, 1137−1155.
(66) Nunomura, N.; Hori, H.; Teranishi, T.; Miyake, M.; Yamada, S. *Phys. Lett. A* **1998**, *249*, 524−530.
(67) Carazzolle, M. F.; Maluf, S. S.; de Siervo, A.; Nascente, P. A. P.; Landers, R.; Kleiman, G. G. *J. Electron Spectrosc.* **2007**, *156*, 405−408.
(68) Massard, R.; Uzio, D.; Thomazeau, C.; Pichon, C.; Rousset, J. L.; Bertolini, J. C. *J. Catal.* **2007**, *245*, 133−143.